REPORT DOCUMENTATION PAGE

AFRL-SR-AR-TR-05-

0137

1. REPORT DATE *(DD-MM-YYYY)*	2. REPORT TYPE	3. DATES COVERED *(From - To)*
	Final	1 Febuary 2002 - 31 December 2004

4. TITLE AND SUBTITLE
High Order Accuracy Methods for the Simulations of Reactive Flows

5a. CONTRACT NUMBER

5b. GRANT NUMBER
F49620-02-1-0113

5c. PROGRAM ELEMENT NUMBER

6. AUTHOR(S)
David Gottlieb

5d. PROJECT NUMBER

5e. TASK NUMBER

5f. WORK UNIT NUMBER

7. PERFORMING ORGANIZATION NAME(S) AND ADDRESS(ES)
Brown University
182 George St.
Providence, RI 02912

8. PERFORMING ORGANIZATION REPORT NUMBER

9. SPONSORING/MONITORING AGENCY NAME(S) AND ADDRESS(ES)
Air Force Office of Scientific Research
4015 Wilson Blvd.
Mail Room 713
Arlington, VA 22203

NM

10. SPONSOR/MONITOR'S ACRONYM(S)
AFOSR

11. SPONSOR/MONITOR'S REPORT NUMBER(S)

12. DISTRIBUTION/AVAILABILITY STATEMENT
Distribution Statement A. Approved for public release; distribution is unlimited.

13. SUPPLEMENTARY NOTES

14. ABSTRACT

Under this grant we have attempted to simulate supersonic reactive flows with high order accuracy methods. The scientific reason for using high order methods is that simulations of supersonicreactive flows require long time integrations and the resolution of fine scales of the flow. It is well known that high order accuracy methods are

20050414 036

15. SUBJECT TERMS

16. SECURITY CLASSIFICATION OF:			17. LIMITATION OF ABSTRACT	18. NUMBER OF PAGES	19a. NAME OF RESPONSIBLE PERSON
a. REPORT	b. ABSTRACT	c. THIS PAGE			David Gottlieb
U	U	U	UU		19b. TELEPHONE NUMBER *(Include area code)*

Final Report: High Order Accuracy Methods for the Simulations of Recative Flows

AFOSR grant F49620-02-1-0113

David Gottlieb

1 Introduction

Under this grant we have attemted to simulate supersonic reactive flows with high order accuracy methods. The scientific reason for using high order methods is that simulations of supersonic reactive flows require long time integrations and the resolution of fine scales of the flow. It is well known that high order accuracy methods are mandatory in satisfying these requirements.

Our main codes are spectral, i.e. based on expansions in global polynomials. The two issues that we have addressed in the last few years are discontinuities and geometrical flexibility. To adapt spectral methods to discontinuities we used low pass filters to stabilize the scheme and a postprocessing of the solution to recover the accuracy. We have resolved the Gibbs phenomenon and showed that a proper postprocessing can recover spectral accuracy in smooth regions of the flow. The theory is not a constructive one in the sense that it does not discuss optimal methods for postprocessing.

A great deal of work has been done in the last decade in adaptive spectral methods to complex domains. The idea here is to use multidomain techniques where spectral methods are used locally at every subdomain. Good sets of collocation points has been found for triangles and tetrahydra, that enable the construction of interpolation polynomials in those subdomains. The main difficulty is the imposition of interface boundary conditions. We have started to study an alternative of the DG method. We look for a discontinuous Collocation method, which is more natural in the framework of spectral methods.

There are uncertainties associate with any aspect of computations of reactive flows. We started to study the effects of uncertainties in initial conditions on the steady state

supersonic flows in the double-throated nozzle using the polynomial chaos expansions. The results obtained are summarized in Section 4.

In the applications part we considered two major applications: The first is simulations of Shock-Induced Turbulence Mixing and the second is the computational study of flame-holders in SCRAMJETs, mainly recessed cavity flameholders. For the first subject the principal research objective has been to develop new state-of-the-art high-order accurate numerical methods for the multi-dimensional numerical simulations of the fully-nonlinear evolution of hydrodynamic instabilities and late-time turbulent mixing generated by single- and multi-mode Richtmyer-Meshkov, Rayleigh-Taylor, and Kelvin-Helmholtz instabilities. This will be discussed in Section 6.

In the second application we considered supersonic combustion problems in recessed cavities in order to establish the efficacy of recessed cavity flame-holders. Recessed cavities provide a high temperature, low speed recirculating region that can support the production of radicals created during chemical reactions. This stable and efficient flame-holding performance by the cavity is achieved by generating a recirculation region inside the cavity where a hot pool of radicals forms resulting in reducing the induction time and thus obtaining the auto-ignition. Experiments have shown that such efficiency depends on the geometry of the cavity such as the degree of the slantness of the aft wall and the length to depth ratio of cavity. This will be discussed in Section 7.

2 Postprocessing Techniques

Sufficient conditions for the removal of the Gibbs phenomenon were given in [38]. Consider a function $f(x) \in L^2[-1,1]$ and assume that there is a subinterval $[a,b] \subset [-1,1]$ in which $f(x)$ is analytic. (For convenience we define the local variable, $\xi = -1 + 2\frac{x-a}{b-a}$ such that if $a \leq x \leq b$ then $-1 \leq \xi \leq 1$.) Let the family $\{\Psi_k(x)\}$, be orthonormal under a scalar product $(\cdot\,,\cdot)$, and denote the finite expansion of $f(x)$ in this basis by $f_N(x)$,

$$f_N(x) \;=\; \sum_{k=0}^{N} (f, \Psi_k)\Psi_k(x).$$

Let the family $\{\Phi_k^\lambda(\xi)\}$ be Gibbs complementary to the family $\{\Psi_k(x)\}$ (see [38] for its exact definition), then the postprocessed reconstruction given by

$$g_N(x) = \sum_{l=0}^{\lambda} < f_N, \Phi_l^\lambda >_\lambda \Phi_l^\lambda(\xi(x))$$

converges exponentially to $f(x)$, i.e.

$$\max_{a\leq x\leq b} |f(x) - g_N(x)| \;\leq\; e^{-qN}, \qquad q > 0.$$

In a series of papers it has been shown that the Gegenbauer polynomials

$$\Phi_k^\lambda(\xi) \quad = \quad \frac{1}{\sqrt{h_k^\lambda}} C_k^\lambda(\xi)$$

which are orthonormal under the inner product $< \cdot, \cdot >_\lambda$ defined by

$$< f, g >_\lambda \quad = \quad \int_{-1}^{1} (1-x^2)^{\lambda - \frac{1}{2}} f(\xi) g(\xi)\, d\xi$$

are Gibbs complementary to all commonly used spectral approximations.

The Gegenbauer method is not robust, it is sensitive to roundoff errors and to the choice of the parameters λ and m. A different implementation of the Gegenbauer postprocessing method has been suggested recently by Jung and Shizgal [53]. To explain the differences between the direct Gegenbauer method and the inverse Gegenbauer method suggested in [53], consider the case of the Fourier expansion of a nonperiodic problem. The Fourier approximation $f_N(x)$ of $f(x)$

$$f_N(x) \quad = \quad \sum_{k=-N}^{N} \hat{f}_k e^{ik\pi x},$$

where $\hat{f}_k = \left(f(x), e^{ik\pi x}\right)$, and we construct

$$f_N^m(x) \quad = \quad \sum_{l=0}^{m} \hat{g}_l C_l^\lambda(x),$$

where $\hat{g}_l =< f_N, C_l^\lambda(x) >_\lambda$. In the Inverse method we use the relationship

$$\hat{f}_k = (f_N^m(x), e^{ik\pi x})$$

and invert to find $\hat{g}_l$. Thus if we define the matrix

$$W_{kl} = (C_l^\lambda(x), e^{ik\pi x})_F = \int_{-1}^{1} (1-x^2)^{\lambda - \frac{1}{2}} C_l^\lambda(x) e^{ik\pi x} dx,$$

and $\hat{f}_k = (f, e^{ik\pi x})$, then

$$\sum_{l=0}^{m} W_{kl} g_l^\lambda = \hat{f}_k.$$

The method seems to be less sensitive to roundoff errors or to the choice of parameters. In particular if the original function is a polynomial, the inverse method is exact.

Another approach for the post processing issue involves rational functions. A rapidly converging approximation to finite Fourier series has been studied by defining a rational function which denominator and numerator are represented in finite Fourier sum. Padé

rational approximations have been considered as one of the popular computational methods of representing functions, especially rapidly converging functions since it was proposed by H. Padé in 1892 [8, 49]. They are generally more efficient than polynomial approximations with a reduced number of operations for the same accuracy [23, 25, 26].

The methods discussed before require the knowledge of the position of discontinuity, however with no knowledge of the singularity, Padé reconstruction recovers back a non-oscillatory solution successfully with a reduced overshoot at the singularity. It is due to the fact that the possible existence of poles of some order for the denominator of Padé approximant allows to give a better approximation to the functions exhibiting singular behaviors such as large gradient and discontinuity.

Geer and his coworkers [26], suggested a way of implementing the rational trigonometric approximations for even or odd 2π-periodic piecewise smooth functions and also a way of applying this method to the solution of the initial boundary value problem heat equation. In their work, Fourier-Padé approximants are defined in a nonlinear way such that the relation between the coefficients of the rational approximations and the Fourier coefficients involves a necessary procedure of calculating the integration of rational functions, which makes the numerical scheme relatively complicated. In [25], Fourier expansion is treated as a Laurent expansion, and using Fourier-Padé rational approach the spectral convergence is obtained up to the discontinuity by subtracting off the jump from the Fourier data, which requires the advance knowledge not only of the position of the singularity, but also the magnitude of the jump.

In our work, we have designed two Fourier-Padé methods considering the general case of piecewise analytic functions with no advance knowledge of the singularity. Simple ways of implementing Fourier-Padé Galerkin and Fourier-Padé collocation methods are developed and applied to simulate the solutions of nonlinear partial differential equations. For the hyperbolic partial differential equations such as Burgers' equation, an initially smooth function can evolve into shock in time for inviscid case and large gradient for viscous case. Therefore the standard spectral simulations exhibit the Gibbs phenomenon that degrade the accuracy of the numerical solutions in time. From accurate Fourier data computed by Fourier method, we applied the Fourier-Padé reconstruction as a post-processing. After the post-processing, the computational results show successful reduction of the non-physical oscillations in the standard spectral solutions of the one dimensional inviscid Burgers' equation and the two dimensional inviscid Boussinesq convection flows. Especially, the numerical results for the Boussinesq convection equation are demonstrated in figures 20 and 23. Further study has to be established to find the optimal relation between the degrees of the polynomial of the Padé approximants and the number of the Fourier coefficients.

3 Multi-Domain Methods

To give spectral methods flexibility to handle complex geometries we advocate the use of multidomain methods with penalty type interface conditions, i.e. the boundary conditions are imposed only in a weak form.

We consider two interface conditions, i.e.

1. *The averaging method*, in which the interface conditions are obtained by averaging the state vectors of the two adjacent domains, and

2. *The Penalty method in conservative form* in which the interface conditions are satisfied only in a weak form, leaving the approximations not necessarily continuous at the interfaces.

In the following we will give the penalty interface conditions for the Euler and Navier-Stokes equations and also show that the averaging method is a subset of the penalty method.

Consider the inviscid part only, in the x-direction in the interval $-1 \leq x \leq 1$, i.e.,

$$\frac{\partial q}{\partial t} + \frac{\partial F}{\partial x} = 0. \tag{1}$$

For simplicity, assume that we have two domains in this interval with the interface at $x = 0$, $q_N^I(x,t)$ denotes the numerical solution in the left domain $x \leq 0$ and $q_M^{II}(x,t)$ in the right domain $x \geq 0$. Note that the numerical solution is composed of two polynomials of different orders. The Legendre spectral penalty method is given by

$$\begin{aligned}
\frac{\partial q_N^I}{\partial t} + \frac{\partial I_N^I F(q_N^I)}{\partial x} &= B(q_N^I(-1,t)) + \\
&\quad \tau_1 Q_N(x)[f^+(q_N^I(0,t)) - f^+(q_M^{II}(0,t))] + \\
&\quad \tau_2 Q_N(x)[f^-(q_N^I(0,t)) - f^-(q_M^{II}(0,t))], \\
\frac{\partial q_M^{II}}{\partial t} + \frac{\partial I_M^{II} F(q_M^{II})}{\partial x} &= B(q_M^{II}(1,t)) + \\
&\quad \tau_3 Q_M(x)[f^+(q_M^{II}(0,t)) - f^+(q_N^I(0,t))] + \\
&\quad \tau_4 Q_M(x)[f^-(q_M^{II}(0,t)) - f^-(q_N^I(0,t))]
\end{aligned} \tag{2}$$

where B is a boundary operator at the end points, i.e., $x = \pm 1$ and I_N^I and I_M^{II} are the Legendre interpolation operators for the left and right domains respectively. . The positive and negative fluxes f^+ and f^- are defined by

$$f^{\pm} = \int S \Lambda^{\pm} S^{-1} dq, \tag{3}$$

with

$$A \equiv \frac{\partial F}{\partial q} = S\Lambda S^{-1}. \tag{4}$$

The Jacobian matrix A is assumed to be symmetric. Λ^+ and Λ^- are the diagonal matrices composed of positive and negative eigenvalues of A respectively. $Q_N(x)$ and $Q_M(x)$ are polynomials of orders N and M respectively such that they are zero at all the collocation points except the interface points $x = 0$ (for example $Q_N(x) = \frac{(1-x)T'_N(x)}{N^2}$, $0 \leq x \leq 1$ where $T_N(x)$ is the Chebyshev polynomial of degree N). The penalty parameters τ_1, τ_2, τ_3 and τ_4 are all constants. Since we are interested only in the interface conditions, we ignore the boundary operator B at $x = \pm 1$. Define the discrete scalar product $(p, q)_N = \sum_{i=0}^{N} p^T(\xi_i) q(\xi_i) \omega_i$. ω_i is the weight in the Gauss-Lobatto-Legendre quadrature formula. With the discrete product, the energy $E(t)$ is defined by $E(t) = (q_N^I(x,t), q_N^I(x,t))_N + (q_M^{II}(x,t), q_M^{II}(x,t))_M$. The stability conditions of penalty parameters are given by the following theorem:

Theorem 1 *The energy is bounded by the initial energy of the system if the following conditions are satisfied ;*

$$\begin{aligned} &2\omega_N^I \tau_1 \leq 1, \quad 2\omega_N^I \tau_2 \geq 1, \quad 2\omega_M^{II} \tau_3 \leq -1, \quad 2\omega_M^{II} \tau_4 \geq -1, \\ &\omega_N^I \tau_1 - \omega_M^{II} \tau_3 = 1, \quad \omega_N^I \tau_2 - \omega_M^{II} \tau_4 = 1. \end{aligned} \tag{5}$$

The penalty method in the case of the 2-D Euler equation is given by

$$\begin{aligned} \frac{\partial q_N}{\partial t} + \frac{\partial I_N F(q_N)}{\partial x} + \frac{\partial I_N G(q_N)}{\partial y} &= \tau_{1,3} Q(x,y)[f^+(q_N) - f^+(q_{M-})] + \\ &\quad \tau_{2,4} Q(x,y)[f^-(q_N) - f^-(q_{M-})], \end{aligned} \tag{6}$$

where q_{M-} is the state vector of the adjacent domain at the interface of degree M, $\tau_{1,3}(\tau_{2,4})$ denotes $\tau_1(\tau_2)$ and $\tau_3(\tau_4)$ respectively. τ_1 and τ_2 (τ_3 and τ_4) are the penalty parameters for the right(left) in x-direction and top(bottom) in y-direction respectively. $Q(x,y)$ is a polynomial which vanishes at all of interior points of the domain and is equal to 1 at the four interfaces. Note that the boundary operator B does not appear in the scheme. Let A be the linearized Jacobian matrix (around a state vector q_0) of two inviscid fluxes

$$A = \left(\frac{\partial F}{\partial q}, \frac{\partial G}{\partial q} \right) \cdot \vec{n}|_{q_0}. \tag{7}$$

where $\vec{n} = (n_x, n_y)$ is the unit outward normal vector. Since the matrix A is symmetric, there exists S such that

$$A = S\Lambda S^{-1}, \tag{8}$$

where Λ is a diagonal matrix composed of eigenvalues of A. Then $A = A^+ + A^-$ and $A^\pm = S\Lambda^\pm S^{-1}$. $\Lambda^\pm$ is defined as in previous section. Splitting A yields

$$f^\pm = A^\pm q_0, . \tag{9}$$

where $f^\pm$ is obtained from the linearized state.

Remark 1 *Since $\vec{n} = (n_x, n_y)$ is taken to be outward normal vector, the stability condition (6) is now given by*

$$\begin{aligned} &2\omega_N^I \tau_1 \leq 1, \quad 2\omega_N^I \tau_2 \geq 1, \quad 2\omega_M^{II} \tau_3 \leq 1, \quad 2\omega_M^{II} \tau_4 \geq 1, \\ &\omega_N^I \tau_1 + \omega_M^{II} \tau_4 = 1, \quad \omega_N^I \tau_2 + \omega_M^{II} \tau_3 = 1. \end{aligned} \tag{10}$$

When dealing with the Navier Stokes equation, we keep the penalty form for the Euler fluxes and add a penalty term for the viscous fluxes. The stability of this procedure stems from the fact that the Jacobian matrices for the full reactive Navier-Stokes equation can be symmetrized by the same similarity transformation (see Appendix_B in [17]). Thus we get the system:

$$\begin{aligned} \frac{\partial q_N}{\partial t} + \frac{\partial I_N F}{\partial x} + \frac{\partial I_N G}{\partial y} \quad = \quad & \frac{\partial I_N F_\nu}{\partial x} + \frac{\partial I_N G_\nu}{\partial y} + \\ & \tau_{1,3} Q(x,y)[f^+(q_N) - f^+(q_{M-})] + \\ & \tau_{2,4} Q(x,y)[f^-(q_N) - f^-(q_{M-})] + \\ & \tau_{6,8} Q(x,y)[\mathbf{A}_\nu \cdot \mathbf{q}_N - \mathbf{A}_\nu \cdot \mathbf{q}_{M-}] + \\ & \tau_{5,7} Q(x,y)[\mathbf{A}_\nu \cdot \partial \mathbf{q}_N - \mathbf{A}_\nu \cdot \partial \mathbf{q}_{M-}]. \end{aligned} \tag{11}$$

Here $f^\pm$ are same as defined in the previous section and the Jacobian matrix vector $\mathbf{A}_\nu$ is given by

$$\mathbf{A}_\nu = \left(\frac{\partial F_\nu}{\partial q_x} n_x, \frac{\partial G_\nu}{\partial q_y} n_y \right) |_{q_0}, \tag{12}$$

and

$$\mathbf{q} = (q, q), \quad \partial \mathbf{q} = (q_x, q_y), \tag{13}$$

where again $\mathbf{q}_-$ and $\partial \mathbf{q}_-$ denote the adjacent domains state vectors and their derivatives. Note that the penalty terms $\mathbf{A}_\nu \cdot \partial \mathbf{q}$ does not appear in [9, 47, 48]. The penalty parameters $\tau_{5,7}$ and $\tau_{6,8}$ are defined in the same way as in the previous section. To seek stable penalty parameters we split the inviscid and viscous fluxes and keep the stability conditions of $\tau_{1,2,3,4}$ for the inviscid flux as in Theorem 1. The stability conditions of $\tau_{5,7}$ and $\tau_{6,8}$ are given in the following Theorem :

Theorem 2 *The penalty method for the Navier-Stokes equations (12) is stable if the penalty parameters τ_j , $j = 1...4$ are as in Theorem 1 and the rest satisfy:*

$$\begin{aligned} \omega_N\tau_6 &\leq 0, \\ \omega_N\tau_6 - \omega_M\tau_8 &= 0, \\ 1 + \omega_N\tau_5 - \omega_M\tau_7 &= 0, \\ \left(\frac{1}{\omega_M} + \frac{1}{\omega_N}\right)\omega_M^2\tau_7^2 - 2\tau_7 + 4\omega_N\tau_6 + \frac{1}{\omega_M} &\leq 0 \end{aligned} \tag{14}$$

in addition to the conditions specified for τ_1, τ_2, τ_3 and τ_4 in Theorem 1.

Note that these conditions are given independently of the local flow properties. And moreover, the penalty parameters of each domain are constrained by its adjacent domain.

Remark 2 *For $\vec{n}$ to be outward normal vector the condition (16) is now given by*

$$\begin{aligned} &\omega_N\tau_6 \leq 0, \quad \omega_N\tau_6 + \omega_M\tau_8 = 0, \quad 1 + \omega_N\tau_5 + \omega_M\tau_7 = 0, \\ &\left(\frac{1}{\omega_M} + \frac{1}{\omega_N}\right)\omega_M^2\tau_7^2 + 2\tau_7 + 4\omega_N\tau_6 + \frac{1}{\omega_M} \leq 0 \end{aligned} \tag{15}$$

with the conditions (11)

The averaging method for the N-S equations can be presented as

$$\begin{aligned} \frac{\partial q}{\partial t} + \frac{\partial F}{\partial x} + \frac{\partial G}{\partial y} &= \frac{\partial F_\nu}{\partial x} + \frac{\partial G_\nu}{\partial y} + \\ &\tau_{1,3}Q(x,y)[f'^{+}(q) - f'^{+}(q_-)] + \\ &\tau_{2,4}Q(x,y)[f'^{-}(q) - f'^{-}(q_-)] + \\ &\tau_{5,7}Q(x,y)[\mathbf{A}_\nu \cdot \partial^2\mathbf{q} - \mathbf{A}_\nu \cdot \partial^2\mathbf{q}_-] + \\ &\tau_{6,8}Q(x,y)[\mathbf{A}_\nu \cdot \partial\mathbf{q} - \mathbf{A}_\nu \cdot \partial\mathbf{q}_-], \end{aligned} \tag{16}$$

where $\partial^2\mathbf{q}$ is the second derivative of q in either x or y direction.

Theorem 3 *If $\tau_1 = \tau_3 = \frac{1}{2}$, $\tau_2 = \tau_4 = \frac{1}{2}$, $\tau_5 = \tau_7 = \frac{1}{2}$, and $\tau_6 = -\tau_8 = -\frac{1}{2\omega_N}$, then the approximation is continuous at the interface and the scheme (17) is stable.*

To ensure the stability of the scheme at some particular collocation points where the solution become singular and unstable, we use the averaging method adaptively at selective grid points. In particular, we switched from the penalty method to the averaging when the following criteria was satisfied:

$$\max\left(\frac{|\rho - \rho_-|}{|\rho + \rho_-|}, \frac{|T - T_-|}{|T + T_-|}\right) \geq C_{ave}, \tag{17}$$

or

$$\frac{|P - P_-|}{|P + P_-|} \geq C_{ave}, \tag{18}$$

where C_{ave} is a non-negative constant. Note that $C_{ave} = 0$ leads to the averaging method, whereas a large C_{ave} results in the penalty method. For the value of C_{ave} used in this paper, we found out that there were very few points in which one needs to switch from the penalty to the averaging procedure. Moreover this happened only at very few time steps.

4 Uncertainty Analysis in Supersonic Flow Problems

It is well known that the steady state of an isentropic flow in a double-throated nozzle is not unique. In fact, the steady state flow can be either completely supersonic or completely subsonic or a flow containing a shock wave connecting the supersonic branch of the solution to the subsonic branch, the location of the shock wave depends uniquely on the initial condition.

In [51] a model equation, having the same features, was considered and analyzed, and in [11] the model has been generalized.

In many applications there are uncertainties involved in the initial conditions and the question arises: what can be said about the shock location if there are uncertainties in the initial conditions. We note that while randomness enters through the initial conditions in this problem, random effects can generally enter into practical problems through boundary conditions, initial conditions, the domain geometry, missing variables and fluid properties etc. Such random effects in the inputs produce stochastic solutions as outputs, requiring new methodologies to model and analyze the impact of such uncertainties. In our case we are interested in the statistics of some derived quantities (e.g., the shock position of a solution). Such are often hard to accurately compute from the first few moments of the solutions.

In a preliminary work, generalized polynomial chaos methods were implemented to compute the probability density function (PDF) of the shock location for the cases where the initial conditions are assumed to be different random processes (fields).

Our preliminary conclusions are:

- Polynomial chaos (PC) expansion modes are smooth functions of the spatial variable x, although the individual solution realizations are discontinuous in the spatial variable x.

- The solution is discontinuous in the random variable space at a fixed point x. Filtering is necessary for the stability of the scheme, because generalized polynomial chaos

methods are spectral representations of the random processes.

- When the variance of the initial condition is small, the probability of the density function (PDF) of the shock locations is computed with high accuracy. Otherwise, many PC expansion terms are needed to produce reasonable results. As first noted by Chorin, this is due to the slow convergence of PC expansions of discontinuous functions in the random fields.

- The biggest absolute eigenvalue of the Jacobi matrix of the system increases quickly with respect to the number of PC terms used in the expansion. This might cause large dissipation for some numerical schemes. The fast increasing size of the system, when using more PC terms, could also be problematic if one wants to solve the system with a high order numerical scheme using characteristic decomposition, e.g., high order ENO or WENO.

The fact that the coefficients in the PC expansion are smooth is surprising. It seems although the solution contains a shock, we can compute it by embedding it in a random space and computing smooth solutions in that space. We plan to study whether this might be a general procedure in computing shock waves.

5 Richtmyer-Meshkov Instabilities

In the mixing of fuel with oxidants in SCRAMJET engine, the fuel jets are under impulsive acceleration by shock waves. The fuel mixing efficiency are enhanced by the stretching of the fuel-oxidants interface and the breakup of fuels into finer droplets. Inertial Confinement Fusion Program (ICF) uses high energy pulse source such as X-ray and laser to illuminate the target sphere in order to achieve auto fusion ignition on the National Ignition Facility. It is crucial to achieve an uniform compression of the target sphere as possible for maximum efficiency as the impulsively accelerated non-uniform sphere surface by a shock wave causes a non-uniform pressure profile over the sphere.

The source of these phenomenon known as Richtmyer-Meshkov Instability is related to the well known fluid instability studied theoretically by Richtmyer and experimentally by Meshkov. The Richtmyer-Meshkov Instability (RMI) results from a impulsively accelerated interface of materials with different densities under perturbation. This form of instability is different than the closely related fluid instability known as the Rayleigh-Taylor instability in which the material interface is under constant acceleration force such as gravity. The vorticity generated by the cross product of the pressure gradient and the density gradient deforms the and amplifies the interface perturbation and grows in time. The penetration of

the heavier fluid into lighter fluid form spike and bubble vice versa. Growth of the interface amplitude and secondary shear instability promote the onset of turbulence mixing and enlarged in time. The RMI is encountered in a variety of physical contexts such as, but not limited to, those described above. Reader are referred to extensive literature available.

In order to capture the shock-interface interaction and the fine scale structures within the turbulence mixing zone, high order methods are highly desirable. Among the high orders schemes considered, Spectral methods (Spectral) and Weighted Essentially Non-Oscillatory finite difference schemes (WENO) are considered in this study. High Order compact scheme is another candidate but was not considered in this study. High order, in the sense, means order of accuracy is at least greater than two. In this study, we devise the algorithms based on the methods mentioned above. To our knowledge, this is probably the first time these high order methods are implemented for the study of the RMI. In order to evaluate the performance of the devised schemes, only single mode interface perturbation will be included in this study.

From the point of view of the numerical calculation, we can break the RMI problem into two parts.

First, we have the issue of reliably calculating the motion of a possibly very strong shock wave, and second we have the issue of reliably calculating the mix that ensues after this shock wave accelerates the interface. It is in this second area of calculating the ensuing mix where high order numerical schemes offer unparalleled efficiency. This efficiency comes from the very fundamental fact that the truncation error in the differentiation operators can be made much smaller by increasing the order of the scheme than by increasing the number of grid points thereby making long-time integration computationally much less expensive with high order schemes.

Secondly, when the flow variables are differentiable and contain significant structure, i.e., when a Fourier representation of the flow variables decays slowly, then the truncation error is again highly favorable to high order schemes.

For these two reasons, if one has structure, with or without shocks, high order schemes are orders of magnitude computationally more efficient than low order schemes. This leads us to the issue of high order schemes in the presence of strong shocks. Of course, if one has only shocks and no structure, then there is no reason for using high order schemes. So, we assume the existence of structure in the flow variables.

When shocks are present, there has been a great deal of technology developed over the last few decades that insures that one can obtain a high order accuracy away from the shock even though the calculation is, as it must be, first order at the shock. Here we explore two such high order schemes, the Weighted Essentially Non-oscillatory (WENO) scheme and spectral methods. The WENO scheme and its predecessor the Essentially

Non-oscillatory (ENO) schemes were designed exactly for problems such as RMI and are extremely robust even for very strong shocks. We would like to stress the importance of comparing numerical results obtained by algorithms based on different philosophy. The confidence of the numerically converged results can be greatly enhanced by their agreements of the numerical results. In our case, spectral methods is global in nature as opposed to the finite difference scheme which is local in nature as seen in the following sections.

In a series of papers [32, 33, 34, 35, 36], it was shown that given the spectral approximation to a piecewise smooth function one can construct an exponentially convergent approximation to the function. This result had been proven for Fourier, Chebyshev, Legendre and spectral methods based on spherical harmonics.

For the ease of presentation, we discuss the results for Fourier approximations, since nothing essential is lost in the Chebyshev case.

The exponential filter offers the flexibility of changing the order of the filter simply by specifying a different γ. One does not have to write a different filter for different order. Thus varying γ with N yields exponential accuracy according to [59].

The above defined filters do not completely remove the Gibbs phenomenon as oscillations still exist in the neighborhood of the discontinuities. In order to recover the full accuracy in any region where the function is continuous, one has to use a different idea. In [35] it is shown how to use a known set of $2N+1$ Fourier coefficients to obtains the coefficients of a different expansion (based on the Gegenbauer polynomials). The new expansion converges *exponentially* in any smooth region.

In practice, when solving differential equations one uses the exponential filter at every time step and the Gegenbauer filter at the end of the calculations as a postprocessor.

When spectral methods are applied to nonlinear hyperbolic equations in conservation form the problem of an entropy satisfying solution arises. In fact, there is no artificial dissipation in the method to indicate that the solution is a limit of a dissipative process. One clearly needs to add artificial dissipation. However this dissipation must be spectrally small in order not to affect the overall accuracy. This problem had been addressed in [56, 57, 44].

It has been shown that with a suitable addition of (spectrally small) artificial dissipation to the high modes only, the method converges. In this paper we used one version of the above idea: the Super Vanishing Viscosity method (SVV) suggested by Tadmor [56, 57].

The interaction between the shock and the interface, generates a shock triple point along the gaseous interface. Localized sharp gradient could cause numerical instability if insufficient localized physical/numerical dissipation existed there. For the Spectral scheme, instabilities were observed in the case of under-resolved simulation and/or using too high

order of the global filtering. Global strong filtering would keep the scheme stable at the cost of smoothing out all fine scale physical structures, which is highly undesirable when resolution of fine scale structures is essential for understanding of the issue of shock induced mixing.

Since this is a local phenomenon, a sufficient strong local dissipation or *Local Adaptive Filtering* would be needed to keep the scheme stable. The location of those collocation points where the density $\rho <= \rho_{tol}$ will first be located and marked for further processing. A global strong filtering, for example $\gamma = 2$ will be used to reduce the magnitude of the oscillations at those points only. In all the cases studied here, ρ_{tol} is set to be $\frac{1}{2}\rho_{min}$ where ρ_{min} is the expected minimal density value, $\rho_{min} = \rho_{Xe}$ for example.

Our experiences with this class of problem indicated that the local adaptive filtering only applied on a few (in the range of 1 to 7) grid points around the shock triple point only as the shock propagated along the gaseous interface in the earlier time. Otherwise, the Spectral scheme remained stable for all other time and no local adaptive filtering is needed.

After the evaluation of the spatial operator, the third order TVD Runge-Kutta scheme of Shu and Osher [54] was used to solve the system of ODE's. It has the form of

$$\begin{aligned}
\vec{U}^1 &= \vec{U}^n + \Delta t L(\vec{U}^n) \\
\vec{U}^2 &= \frac{1}{4}(3\vec{U}^n + \vec{U}^1 + \Delta t L(\vec{U}^1)) \\
\vec{U}^{n+1} &= \frac{1}{3}(\vec{U}^n + 2\vec{U}^2 + 2\Delta t L(\vec{U}^2)) .
\end{aligned}$$

L is the spatial operator. $\vec{U}^n$ and $\vec{U}^{n+1}$ are the data arrays at the n-th and $(n+1)$-th time step, respectively. $\vec{U}^1$ and $\vec{U}^2$ are two temporary arrays at the intermediate Runge-Kutta stages. The scheme is stable for CFL < 1. This Runge Kutta scheme is a low storage scheme as it can be rewritten in such a way that only two arrays $\vec{U}^n$ and $\vec{U}^1$ are needed.

We summarize the overall solution procedures of the algorithm as follow,

- Periodical Domain is specified in the y direction and symmetry property of the problem is exploited to reduce the amount of computational operations by half.
- Spatial Algorithm :
  1. Combined Chebyshev (x) and Fourier (y) collocation method (Spectral),
     - Differentiation and Smoothing operations are performed via an optimized library PseudoPack [13];
     - A 10'th and 9'th order exponential filter used for the differentiation and solution smoothing respectively;

- Kosloff-Tal-Ezer mapping [24, 21] for the Chebyshev collocation methods.
- An adaptive local smoothing.

2. Fifth order WENO finite difference scheme (WENO-LF-5) with Lax-Frederick flux splitting.

- The third order TVD Runge Kutta method by Shu and Osher [54] is used to advance the solution in time.

A series of numerical simulations are carried out to investigate the convergence properties of both the Spectral scheme and the WENO scheme. Simulations, using various interface thicknesses and resolutions, are computed and terminated at some representative time after the shock had transmitted sufficiently far away from the interface and before exiting the physical domain. It allows the development of vortical rollups of the gaseous interface. Vorticities are generated by the cross product of the pressure gradient of the shock and the density gradient of the gases. The final time is set to $t = 50 \times 10^{-6}s$ for $L_x = 50\ cm$ and $t = 143 \times 10^{-6}s$ for $L_x = 150\ cm$.

As evidenced from the results of the Spectral and the WENO calculations shown below, the following major features of the Richtmyer-Meshkov instability can be observed (see figure 3) at time $t = 50 \times 10^{-6}s$, namely,

- Wave generated by the shock refraction behind the gas interface in Box 1.
- The penetration of the heavy (Xe) to light (Ar) fluid causes the deformation of the interface into a large mushroom shape structures in Box 2 and the opposite in Box 5. They are referred as Spike and Bubble respectively, in the literatures. They move in the opposite direction relative to each other and form a ever larger turbulence mixing zone.
- Pressure wave along the transmitted shock in Box 3.
- A small jet and its vortical structure located in Box 4. The contact discontinuity develops into a more complicated vortical rollups in a finer and long term simulation possibly caused by the Kelvin-Helmholtz instability.
- Vortical rollups of the gaseous interface inside Box 6.

The global large and median features (Box 1, 2, 3, 4 and 5) are well captured accurately by both numerical schemes for a given resolution. It is unclear, however, if the smaller rollups along the gases interface (Box 6) presented in the high resolution/high order cases are physical due to the non-dissipative nature of the Euler equations or numerical due to

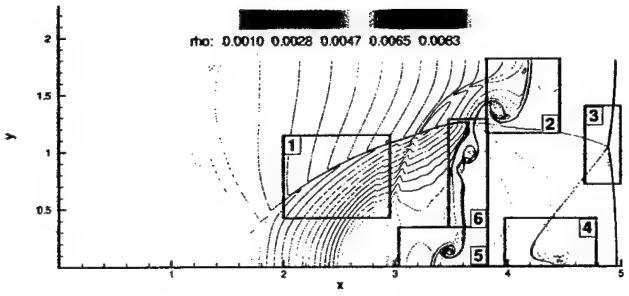

Figure 1: The numbered regions enclose the most prominent flow features of the Richtmyer-Meshkov instability at time $t = 50 \times 10^{-6} s$.

the oscillatory nature of the numerical schemes or both. More researches are needed to answer this question fully.

We shall first examine the convergence property of both the Spectral scheme and the WENO-LF-5 finite difference scheme. For this, we used a thicker interface with $\delta = 0.6\ cm$ to establish the convergence of the numerical schemes of the large and medium scale structures (box 1, 2, 3, 4 and 5 in figure 3). This avoids the possible contamination of numerical artifacts due to high gradients generated along the shock-interface interaction and bypass the issue of under-resolved fine scale physical structures. Furthermore, the spectral solutions are not post-processed by any existing post-processing algorithms to remove the Gibbs oscillations.

Convergence Study : $\delta = 0.6\ cm$

The density ρ and velocity V of the solution of the Spectral and WENO-LF-5 runs are shown in figure 4 at time $t = 50 \times 10^{-6}\ s$ with various resolutions.

It can observed that the large and medium scale structures such as the transmitted shock, the location of the triple point, the shocked-interface velocity, pressure waves and vorticity generation, are basically in excellent agreement with each others. The weak vertical wave located downstream behind the interface is an left over entropy wave from the initial shock condition.

Convergence Study : $\delta = 0.2\ cm$

The interface thickness is further reduced significantly from $\delta = 0.6\ cm$ to $\delta = 0.2\ cm$. The density ρ and velocity V of the solution of the Spectral and WENO-LF-5 runs are shown in figures 5 and 6 respectively, at time $t = 50 \times 10^{-6}\ s$ with various resolutions.

Similar to the previous case of $\delta = 0.6\ cm$, it can be observed that the large and median

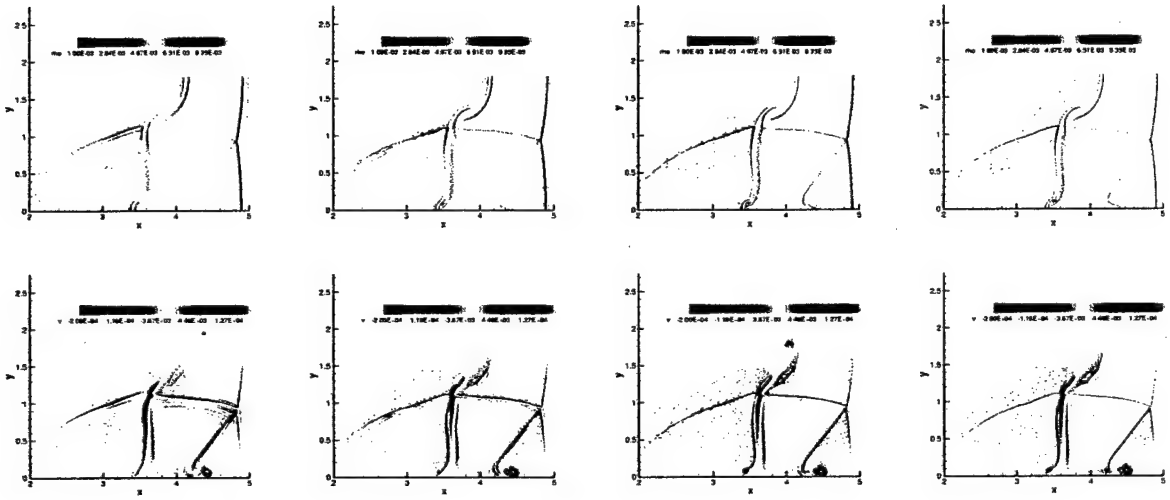

Figure 2: Convergence Study $\delta = 0.6\ cm$: Density (Top Row) and V-Velocity (Bottom Row) contour plot of the Richtmyer-Meshkov instability as computed by the Spectral scheme and the WENO-LF-5 scheme. Domain length in x is $L_x = 5\ cm$. The interface thickness $\delta = 0.6\ cm$. The final time is $t = 50 \times 10^{-6} s$. The resolution of the Spectral schemes are 256x128 (Top Left), 512x256 (Top Right) and 1024x512 (Bottom Left) and the WENO scheme is 1024x512 (Bottom Right).

scale structures such as transmitted shock, shocked-interface velocity and shock triple point are basically in excellent agreement with each others. Some discrepancies of the fine scale structures along the gaseous interface, as can be expected for numerical simulation of the Euler equations which is sensitive to perturbation in nature, are observed.

Snapshot of the evolution of density and velocity flow fields at several immediate times are illustrated in figure (7), for the Spectral scheme and in figure (7) for the WENO scheme. The contour levels are the same and constant for both schemes in all plots.

The Mach number M, the Atwood number At and the interface curvature play an important role on the growth of perturbed amplitude on the interface. In the particular set of parameters studied here with high Mach number $M = 4.46$ and median Atwood number $At \approx 0.54$, a formation of triple-shock configuration along the interface indicates that shock-interface interaction is in the "hard" regime. A "hard" regime, as quoted from Zaytsev etc. is "the propagation of secondary shocks across the flow that is accompanied by the formation of breaks and triple configurations on the refracted and reflected shocks". The triple-shock formation can be observed easily in the early time $<\approx 30 \times 10^{-6} s$.

As the Mach number increases, high order schemes tend to break down as the solution develops singularity and/or high gradients in time in which the numerical schemes becomes more difficult to resolve them. For the spectral methods, we have developed a Spectral

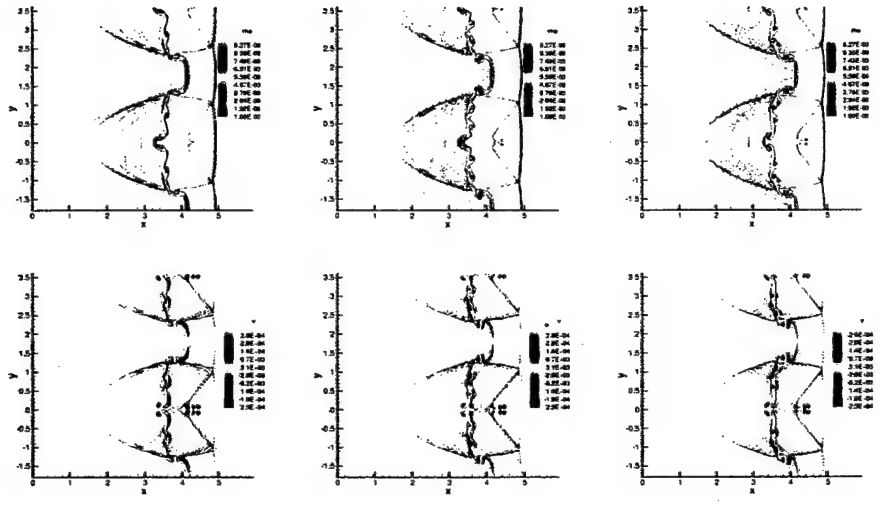

Figure 3: Convergence Study $\delta = 0.2\ cm$: Density (Top Row) and V-Velocity (Bottom Row) contour plot of the Richtmyer-Meshkov instability as computed by the Spectral scheme. Domain length in x is $L_x = 5\ cm$. The interface thickness $\delta = 0.2\ cm$. The final time is $t = 50 \times 10^{-6} s$. The resolution of the Spectral schemes are 384x192 (Top Left), 512x256 (Top Right) and 1024x256 (Bottom Left).

Adaptive Domain Algorithm which adjusts the size of the computational domain in time in order to resolve the fine scale structures at high Mach number as they are developing in time. In figure (8), we presents the density for the Richtmyer-Meshkov instability for the case similar to the previous section except that the Mach number is increased from Mach 4.46 to Mach 10.

In figure 9 we show the preliminary result of the density isosurface plot of the RMI with a Mach 4.46 shock and a three dimensional random pertubation interface separating the Argon and Xenon gases.

6 Recessed Cavity Flameholders

Recessed cavities provide a high temperature, low speed recirculating region that can support the production of radicals created during chemical reactions. This stable and efficient flame-holding performance by the cavity is achieved by generating a recirculation region inside the cavity where a hot pool of radicals forms resulting in reducing the induction time and thus obtaining the auto-ignition [6, 61]. Experiments have shown that such efficiency depends on the geometry of the cavity such as the degree of the slantness of the aft wall and the length to depth ratio of cavity L/D. Thus one can optimize the flame-holding performance by properly adjusting the geometrical parameters of the cavity flame-holder system

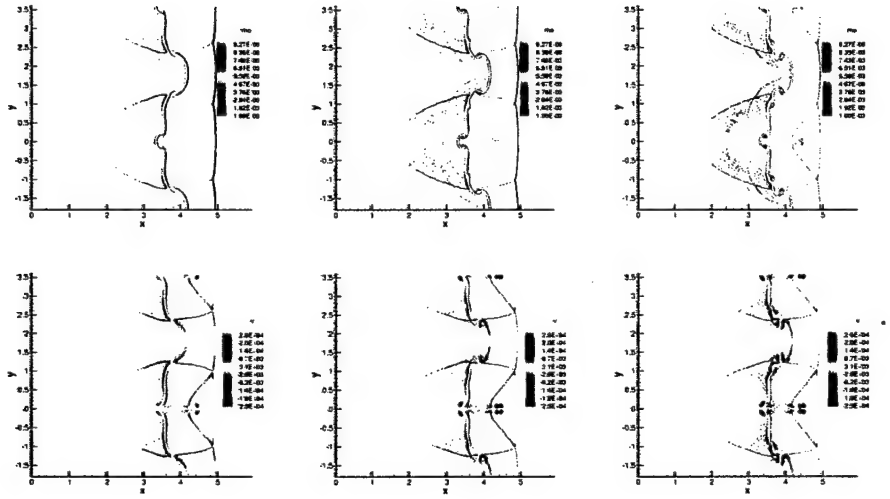

Figure 4: Convergence Study $\delta = 0.2\ cm$: Density (Top Row) and V-Velocity (Bottom Row) contour plot of the Richtmyer-Meshkov instability as computed by the WENO-LF-5scheme. Domain length in x is $L_x = 5\ cm$. The interface thickness $\delta = 0.2\ cm$. The final time is $t = 50 \times 10^{-6} s$. The resolution of the WENO-LF-5 schemes are 256x128 (Top Left), 512x256 (Top Right) and 1024x512 (Bottom Left).

for a given supersonic flight regime. There are two major issues of such cavity flame-holder system that need to be investigated ; (1) *What is the optimal angle of the aft wall for a given L/D?* and (2) *How does the fuel injection interact with cavity flows?* An answer to these questions require both a comprehensive laboratory and numerical experiments.

Results of several numerical studies have shown that the stability of the recirculation inside cavity is enhanced for the lower angle of cavity compared to the rectangular cavity. The present study, however, gives more accurate and finer details of the fields than those done by lower order numerical experiments. We show that a stationary recirculation region is not formed inside the cavity contrary to what the lower order schemes predict. A quantitative analysis made in this study shows that the lower angled wall of the cavity reduces the pressure fluctuations significantly inside the cavity for the non-reactive flows. We obtained a similar result for the reactive flows with the ignition of the fuel supplied initially in the cavity.

In the SCRAMJet community, a cavity with the length-to-depth ratio $L/D < 7 \sim 10$ is usually categorized as an 'open' cavity since the upper shear layer re-attaches at the back face [6]. In this work, we choose the L/D of the baseline cavity to be 4 and thus the open cavity system is considered. The coordinates of the cavity are $(7cm, -1cm)$ for the upper left and $(11cm, -2cm)$ for the right bottom corners of cavity. With the length of the neck of the cavity fixed to be $4cm$, we consider three different angles of the right corner

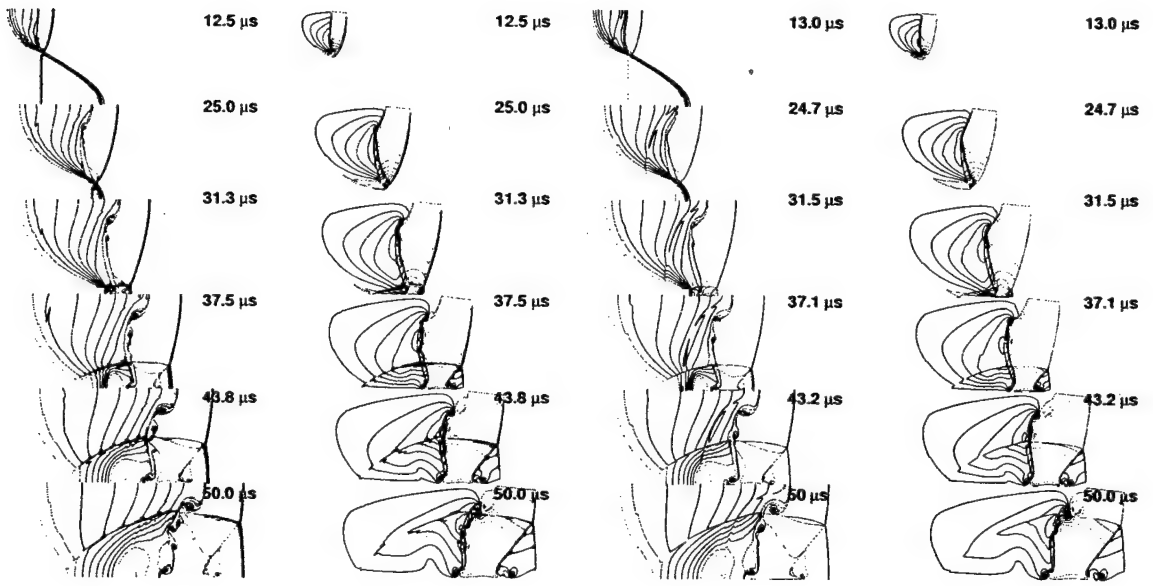

Figure 5: Snapshot of evolution with the Spectral (Leftmost two figures) and WENO-LF-5 (Rightmost two figures) schemes and $\delta = 0.2\ cm$:
In the leftmost two figures (Spectral), the Density (Left) and Velocity (Right) contour plot of the Richtmyer-Meshkov instability as computed by the Spectral scheme at time $t = 12.5 \times 10^{-6}s, 25.0 \times 10^{-6}s, 31.3 \times 10^{-6}s, 37.5 \times 10^{-6}s, 43.8 \times 10^{-6}s$ and $50.0 \times 10^{-6}s$ are showed. The resolution of the Spectral scheme is 1024x256.
In the rightmost two figures (WENO-LF-5), the Density (Left) and Velocity (Right) contour plot of the Richtmyer-Meshkov instability as computed by the WENO-LF-5 scheme at time $t = 13.0 \times 10^{-6}s, 24.7 \times 10^{-6}s, 31.5 \times 10^{-6}s, 37.1 \times 10^{-6}s, 43.2 \times 10^{-6}s$ and $50.0 \times 10^{-6}s$ are shown. The resolution of the WENO-LF-5 scheme is 1024x512.
Domain length in x is $L_x = 5\ cm$. The interface thickness $\delta = 0.2\ cm$.

of the floor of the cavity (60, 45 and 30), we then compare each one with the case of the rectangular aft wall. The fluid conditions are given as followings; the free stream Mach number $M = 1.91$, total pressure $P = 2.82(atm)$, total temperature $T = 830.6(K)$ and normalized Reynolds number $R_e = 3.9 \times 10^7(1/m)$. Note that the Reynolds number is here normalized and has a unit of $1/[length]$, also the Reynolds number based on the cavity dimensions is $O(10^5)$. The boundary layer thickness scale is $\delta = 5 \times 10^{-4}(m)$, and finally, the wall temperature is $T_w = 460.7835(K)$. The initial configuration for the baseline cavity system is shown in figure 10.

We have conducted two different experiments for each of the following cases : (1) *non-reacting cold flow*, and (2) *reacting flow* . We use 9 and 17 subdomains for both cases 1 and 2. For the outflow conditions at the exit of the system and at the upper boundary, we mainly use a semi-infinite mapping in order to reduce the possible reflections at the

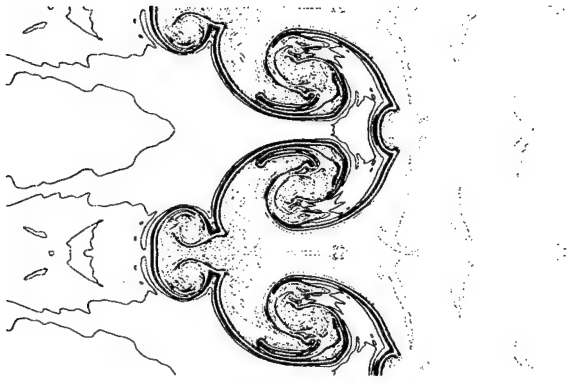

Figure 6: High Mach number case $\delta = 0.2\ cm$: Density contour plot of the Richtmyer-Meshkov instability as computed by the Spectral scheme. The Mach number M=10. Domain length in x is $L_x = 30\ cm$. The interface thickness $\delta = 0.2\ cm$. The final time is $t = 125 \times 10^{-6} s$. The resolution of the Spectral schemes are 2304x256.

boundaries. The characteristic boundary conditions are also applied and will be discussed in the next section and compared to the mapping. For the case of the reactive flows, the cavity was initially filled with Hydrogen fuel with fuel-to-total gas ratio of 0.5. The order of the polynomial of approximation in y direction in the domain beside the wall is taken large enough to resolve the boundary layer well. Finally the adaptive filtering is turned on if the mass fraction of Hydrogen and Oxygen exceed the range of $-0.09 \leq f_{H_2} \leq 1.09, -0.02 \leq f_{O_2} \leq 0.25$ and the temperature exceeds the range of $300(K) \leq T \leq 3500(K)$. As the shear layer and the complex features of the flows develop, the adaptivity criteria for applying the local smoothing is satisfied at some points. In the calculations, we use the 3rd and 2nd order local filtering for the non-reactive and reactive flows respectively. It turns out that the local smoothing was applied in very few points at the upper corner of the cavity wall.

For the adaptive averaging, we use the criteria constant C_{ave} such that the difference of the state vectors (or pressure) between the two adjacent domains is less than 10%. In figure 11 the Penalty Navier-Stokes equations were considered for the non-reactive cold flows. As evident from the contours of the density, the approximations were well matched at the interfaces. Here the outer boundary was approximated by using the characteristic conditions of the inviscid fluxes. The adaptive averaging, with the given adaptivity conditions above, took place at only a few points. The characteristic boundary conditions using the inviscid fluxes yield good results for both the problems of the density peak propagation and the non-reactive cold flows. As in figure 1, we observe that there exist

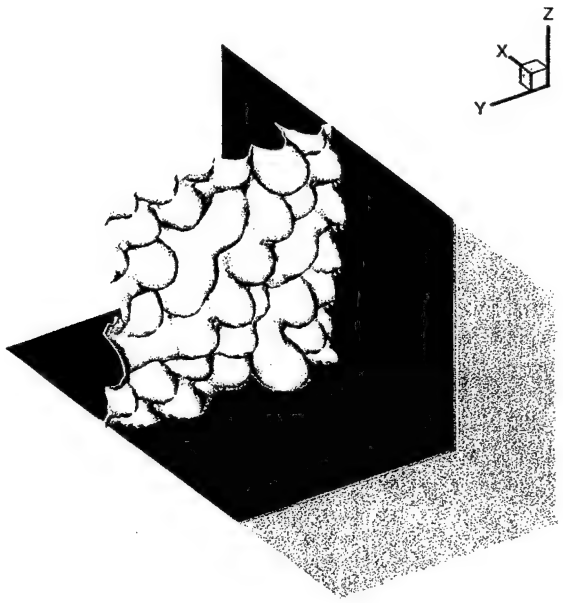

Figure 7: Density isosurface plot of the RMI with a Mach 4.46 shock and a three dimensional random perturbation interface. The gases are the Argon and Xenon

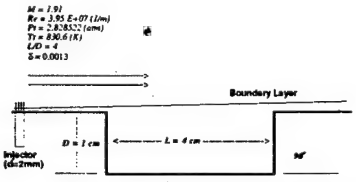

Figure 8: *The initial configuration for the baseline cavity system.*

penalty parameters satisfying the stability conditions that may induce reflecting modes at the interfaces. Figure 12 shows the pressure history of the non-reactive cold flows for the various angles of the aft wall at two different locations inside the cavity, i.e. at the center, $(x, y) = (8.5cm, -1.5cm)$, and at the middle of the floor $(x, y) = (8.5cm, -1.9cm)$.

These figures show that the pressure fluctuations in cavities with lower angle of the aft are weaker than in cavities with higher angles. It is also shown that the attenuation of the pressure fluctuations are obtained both at the center and the middle of the floor of the cavity. It is interesting to observe that the patterns of the pressure fluctuations for a given angle at different locations are different depending on the angle. In the case of the 30 degree aft wall, the pressure fluctuations are almost the same at the two locations considered whereas the case of 45 degree shows a difference in the patterns of the pressure

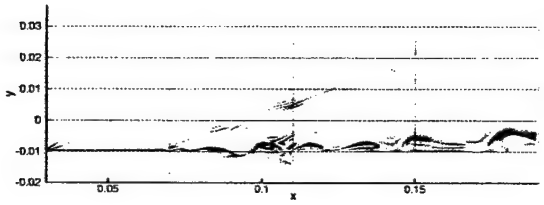

Figure 9: *The non-reactive cold flows with the penalty Navier-Stokes equations: the density contours are given in this figure at $t = 0.25ms$. 17 domains are used and the boundaries of each domain are shown.*

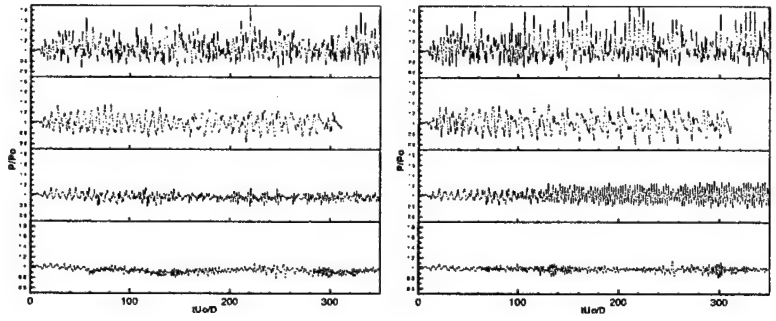

Figure 10: *Pressure history for non-reactive flows: the left panel represents the pressure history at the center of the cavity and the right panel at the middle of the floor of the cavity. Each panel shows the case of 90, 60, 45 and 30 degree cavity walls from top to bottom.*

fluctuations between the two locations. The pressure fluctuations at the bottom grows greater than that at the center after some time.

Figure 13 shows the pressure history when the heavy global filter is applied (in this case, the 4th order filter was used). Unlike the previous case illustrated in figure 12, where the 6th order global filter is used, the pressure fluctuations eventually decay out and a large recirculation zone is formed inside the cavity without any severe pressure fluctuations. Note that the scale in the left panel shown is the same as in figure 12 while the right panel is shown in a smaller scale for a closer look. This figure shows that the large recirculation zone(s) formed inside the cavity obtained by the lower order numerical scheme is induced not physically but rather artificially due to the heavy numerical dissipations. This is clearly shown in figure 14. In this figure a large recirculation zone is observed - this zone is formed earlier than this streamlines are captured - when the 4th order filter is used(left figure) and an almost steady state is already reached as the pressure history indicates in figure 13. We find from the numerical results that the large recirculation is very stable once it forms. This large recirculation and the steady state solutions are not observed in the case

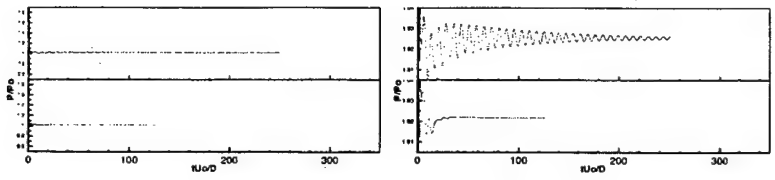

Figure 11: *Pressure history of the non-reactive flows with the use of the 4th order filter: the left panel represents the pressure history at the center of cavity and the right panel shows the left panel in a smaller scale. Each panel shows the case of 90, and 30 degree cavity walls from top to bottom. Note that the scale of the right panel is different from the left.*

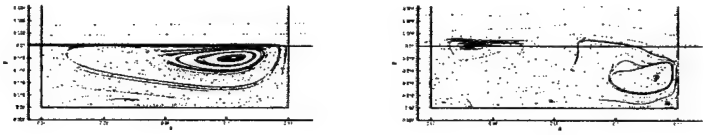

Figure 12: *Streamlines: the left figure shows the streamlines at* $t = 1.685ms$ *for the global filtering order* $\gamma = 4$ *and the right at* $t = 2.38ms$ *for* $\gamma = 6$.

of $\gamma = 6$(right). For the case of $\gamma = 6$ instead of the large single recirculation zone, smaller scale vortex circulations are formed and they are interacting with each other, never reaching the steady state with time. This result shows that for these sensitive problems, high order accuracy should be used in order to minimize the effect of the numerical dissipation.

Figure 15 shows the case of the reactive flows for the 90 and 30 degree aft walls. Similar features of the pressure fluctuations are shown as in the non-reactive flows. However the pressure fluctuations are much more attenuated for both the 90 and 30 degree walls than in the non-reactive cold flows. In the reactive cases Hydrogen fuel, which was initially supplied inside the cavity was consumed. As time elapses, the fuel is consumed out with the production of the water for these cases.

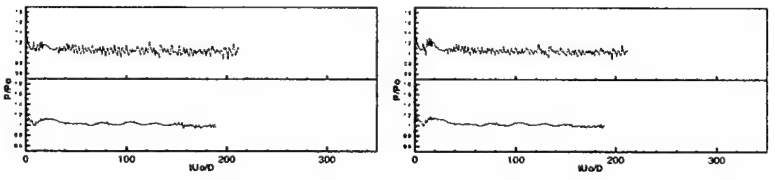

Figure 13: *Pressure history for reactive flows: the left panel represents the pressure history at the center of cavity and the right panel at the middle of the floor of cavity. Each panel shows the case of 90 and 30 degree cavity walls from top to bottom.*

These results demonstrate that simulations of cold flows do not necessarily shed light

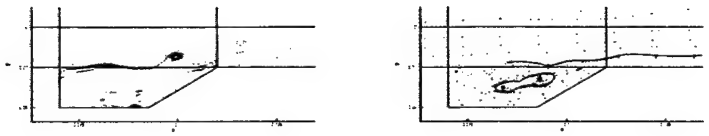

Figure 14: *The water contour of the reactive flows: the left the water density contour is given in the left figure and its streamlines in the right figure at* $t = 0.135ms$.

on the behavior of reactive flows.

Figure 17 shows the density contours and streamlines for the 90, 60, 45 and 30 degree walls at the instant time $t = 2.4ms$. As shown in the figure, the shear layer is becoming weaker as the degree of angle of the aft wall and the flow fields are becoming more regularized for the case of the lower angle. And note that the density compression at the corner of the aft wall is also becoming weaker for the more slanted wall cases.

Reactive flow

Figure 18 shows the water contour inside the cavity for the different angles at different time. Here we define the region where the flames are generated to be same as the region where the water is produced. As the Hydrogen fuel is consumed, the water is produced and starts to be expelled from the cavity to the main channel. The flame-holding efficiency is enhanced if the chemical radicals (water in this case) are stably circulating and long lasting before they are expelled from the cavity. Figure 18 shows that the lower angled aft wall (30 degree in this case) maintains more water than the 90 degree wall at a given time. The figure also shows that the lower angled aft wall holds the flame (water in this case) longer than the 90 degree wall - in the last figure in figure 18 at $t = 2.26ms$, the most water is expelled and the only the small amount is left in the left corner while the 30 degree wall cavity holds the water still through the cavity. These results imply that the flame-holding efficiency can be increased by lowering the angle of the aft wall of the cavity.

Figure 19 shows the streamlines corresponding to the each case of figure 18. Note that compared to the non-reactive cases, the shear layers are less developed for the reactive cases. As the figures of the pressure fluctuation history and figure 19 indicate, the shear layers are weak for both the 90 and the 30 degree walls in the reactive cases.

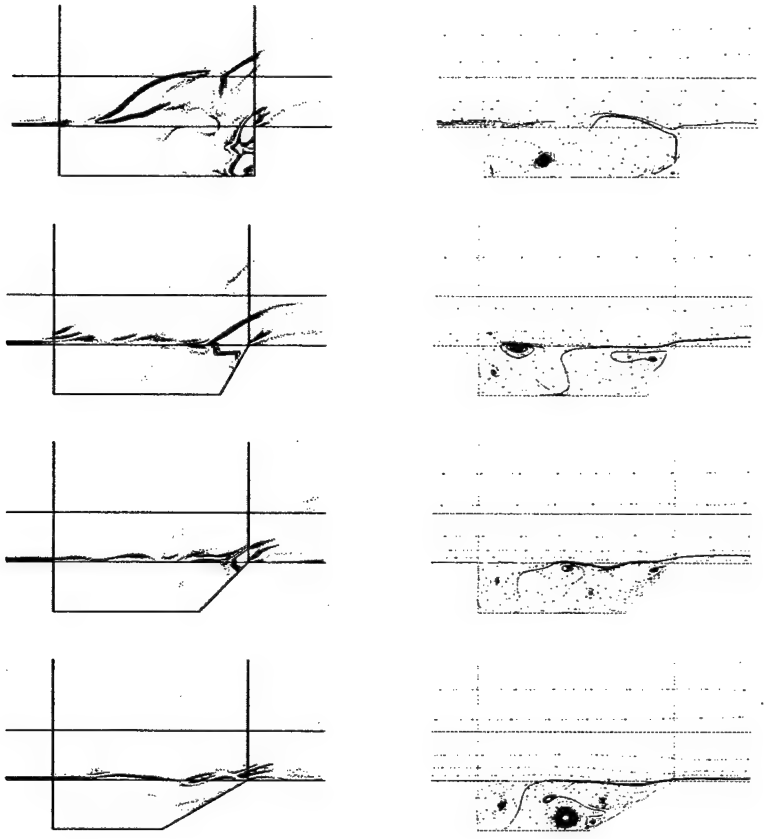

Figure 15: *The density contour and the streamline of the non-reactive flows: the left column shows the density contour for 90, 60, 45 and 30 degree walls from top to bottom and the right column shows the corresponding streamlines at* $t = 2.43ms$. *The maximum contour level is* 1.8 *and the minimum* 0.5 *with the level step size* 50.

References

[1] S. Abarbanel, D. Gottlieb, E. Tadmor, *Spectral methods for discontinuous problems*, in "Numerical Methods for Fluid Dynamics II", ed. by N. W. Morton and M. J. Baines, Oxford University Press, pp. 128-153 (1986)

[2] A. N. Aleshin, E. I. Chebotareva, V. V. Krivets, E. V. Lazareva, S. V. Sergeev, S.N. Titov S. G. Zaytsev, *Investigation of Evolution of Interface After Its Interaction With Shock Waves*, Report No. 06-96, LANL.

[3] G. K. Batchelor, *The stability of a large gas bubble moving through a liquid*, J. Fluid Mech. 184, 399 (1987).

[4] R. H. Bartels, G. W. Stewart, *Algorithm 432, solution of the matrix equation* $Ax + xB = C$, Comm. ACM 15, pp. 820-826 (1972)

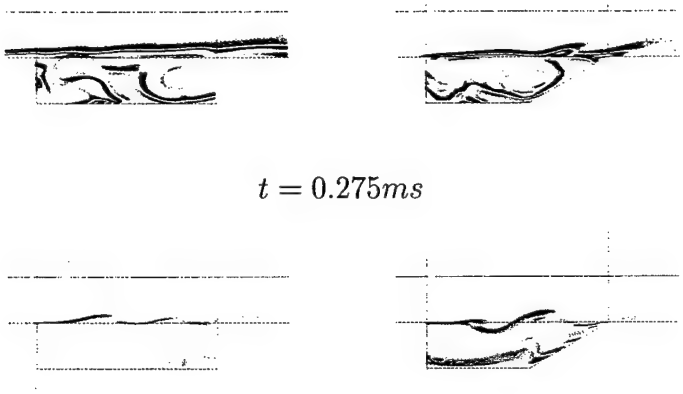

Figure 16: *The water contour of the reactive flows: the water density contours are given in the left figures for 90 degree wall and 30 degree wall in the right figures. From top to bottom the instant times t are* $0.275ms$ *and* $2.26ms$*. The maximum and minimum contour levels are 0.01 and 0.23 respectively with the number of levels* 50.

[5] J. T. Beale, T. Kato, A. Majda, *Remarks on the breakdown of smooth solutions for the 3-D Euler equations* Comm. Math Phys 94, 61 (1984).

[6] A. Ben-Yakar, R. K. Hanson, *Cavity flameholders for ignition and flame stabilization in scramjets - Review and experimental study*, American Institute of Aeronautics and Astronautics, 98-3122 (1998)

[7] M. E. Brachet, D. I. Meiron, S. A. Orszag, B. G. Nickel, R. H. Morf, U. Frisch *Small-scale structure of the Taylor-Green vortex*, J. Fluid Mech., **130**, pp. 411-452 (1983).

[8] H. Cabannes, *Padé approximants method and its applications to mechanics,* Lecture notes in physics edited by J. Ehlers, K. Hepp, H. A. Weidenmüller, J. Zittartz, Springer-Verlag, New York, 1976.

[9] M. H. Carpenter, J. Nordström, D. Gottlieb, *A Stable And Conservative Interface Treatment of Arbitrary Spatial Accuracy*, Journal of Computational Physics, 148-2, pp. 341-365 (1999)

[10] M. H. Carpenter, D. Gottlieb, C. W. Shu, *On the conservation and convergence to weak solutions of global schemes*, ICASE 2001-44 (2001)

[11] C. M. Dafermos, *Trend to Steady State in a Conservation Law with Spatial Inhomogeneity*, Quarterly of Applied Mathematics, Vol. XLV, No. 2 (1987)

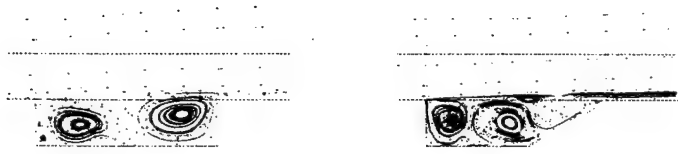

$t = 0.275ms$

$t = 2.26ms$

Figure 17: *The streamlines for the reactive flows: the streamlines for 90 degree wall are shown in the left figures and the 30 degree wall in the right. From top to bottom the times t are* $0.175ms$, $0.275ms$, $0.945ms$ *and* $2.51ms$.

[12] W. S. Don, *Numerical Study of Pseudospectral Methods in Shock Wave Applications*, Journal of Computational Physics, **110**, pp. 103-111 (1994)

[13] W. S. Don, B. Costa, *PseudoPack 2004 : Numerical Library for Pseudospectral Differentiation*, `http://www.cfm.brown.edu/people/wsdon/home.html`

[14] W. S. Don, C. Quillen, *Numerical simulation of Reactive Flow, Part I : Resolution*, Journal of Computational Physics **122**, pp. 244-265 (1995)

[15] W. S. Don, D. Gottlieb, *High Order Methods for Complicated Flows Interacting with Shock Waves*, AIAA 97-0538 (1997)

[16] W. S. Don, D. Gottlieb, *Spectral Simulations of Supersonic Reactive Flows*, SIAM, Journal of Numerical Analysis, **35**, No. 6, pp. 2370-2384 (1998)

[17] W. S. Don, D. Gottlieb, J. H. Jung, *A multi-domain spectral method for supersonic reactive flows*, Journal of Computational Physics, submitted for publication.

[18] W. S. Don, D. Gottlieb, J. H. Jung, *Multi-domain spectral method approach to supersonic combustion of recessed cavity flame-holders*, JANNAF 38th Combustion, 26th Airbreathing Propulsion, 20th Propulsion Systems Hazards, and 2nd Modeling and Simulation Subcommittees Joint Meeting, held in Destin, FL 8-12 April 2002

[19] W. S. Don, D. Gottlieb, C. W. Shu, *High Order Numerical Methods for the Two Dimensional Richtmyer-Meshkov Instability, Part I.*, Conference proceeding for the International Workshop for the Physics of Compressible Turbulence Mixing, Laser and Particle Beams, to appear.

[20] W. S. Don, D. Gottlieb, C. W. Shu, O. Schilling, L. Jameson, *Convergence Study of Inviscid Taylor-Green Vortex Flow* J. Scient. Comput. accepted for publication.

[21] W. S. Don, A. Solomonoff, *Accuracy Enhancement for Higher Derivatives using Chebyshev Collocation and a Mapping Technique*, SIAM J. Sci. Comp. **18**, No. 3 (1997)

[22] A. Dold, B. Eckmann, *Padé approximation and its application*, Springer-Verlag, Berlin Heidelberg, New York, 1979.

[23] L. Emmel, S. M. Kaber, Y. Maday, *Padé-Jacobi filtering for spectral approximations of discontinuous solutions* accepted for publication in Numerical Algorithms, 2002.

[24] D. Kosloff, H. Tal-Ezer, *Modified Chebyshev Pseudospectral Methods With $O(N^{-1})$ Time Step Restriction*, J. Comp. Physics **104**, pp. 457-469 (1993)

[25] T. A. Driscoll, B. Fornberg, *Padé algorithm for the Gibbs phenomenon,* submitted for publication in Numerical Algorithms, 2000.

[26] J. F. Geer, *Rational trigonometric approximations using Fourier series partial sums*, Journal of Sci. Comp., **10**, No. 3 (1995)

[27] J. Gibbs, *Fourier's series*, Letter in Nature, 59, pp. 200 (1898).

[28] D. Gottlieb, M. Y. Hussaini, S. A. Orszag, *Introduction: Theory and Applications of Spectral Methods*, in Spectral Methods for Partial Differential Equations, R. Voigt, D. Gottlieb and M.Y. Hussaini, ed. SIAM, Philadelphia, pp. 1-54 (1984)

[29] D. Gottlieb, L. Lustman, S. A. Orszag, SISC 2, 296 (1981)

[30] D. Gottlieb, L. Lustman, C. L. Streett, *Spectral Methods for Two Dimensional Flows*, in Spectral Methods for PDEs, (SIAM, Philadelphia 1984).

[31] D. Gottlieb, S. A. Orszag, *Numerical Analysis of Spectral Methods: Theory and Applications*, CBMS conference Series in Applied Mathematics **26**, SIAM, (1977).

[32] D. Gottlieb, C. W. Shu, A. Solomonoff, H. Vandeven, *On the Gibbs phenomenon I: recovering exponential accuracy from the Fourier partial sum of a non-periodic analytic function*, J. Comp. and Appl. Math. **43**, pp. 81-98 (1992)

[33] D. Gottlieb, C. W. Shu, *Resolution properties of the Fourier method for discontinuous waves*, Computer Meth. in Appl. Mech. and Eng. **116**, pp. 27-37 (1994)

[34] D. Gottlieb, C. W. Shu, *On the Gibbs phenomenon III: recovering exponential accuracy in a sub-interval from a spectral partial sum of a piecewise analytic function*, S. Num. Anal. **33**, pp. 280-290 (1996)

[35] D. Gottlieb, C. W. Shu, *On the Gibbs phenomenon IV: recovering exponential accuracy in a sub-interval from a Gegenbauer partial sum of a piecewise analytic function*, Math. Comp. **64**, pp. 1081-1095 (1995)

[36] D. Gottlieb, C. W. Shu, *On the Gibbs phenomenon V: recovering exponential accuracy from collocation point values of a piecewise analytic function*, Numerische Mathematik **71**, pp. 511-526 (1995).

[37] D. Gottlieb, C. W. Shu, *The Gibbs phenomenon and its resolution*, SIAM review, 39, pp.644-668, 1997.

[38] D. Gottlieb, C. W. Shu, *General theory for the resolution of the Gibbs phenomenon*, Accademia Nazionale Dei Lincey, ATTI Dei Convegni Lincey 147, pp. 39-48 (1998)

[39] S. Gottlieb, D. Gottlieb, C. W. Shu, to appear.

[40] L. Jameson, *High Order Methods for Resolving Waves: Number of Points per Wavelength*, SIAM J. Sci. Comp. **15**, No. 4 (2000)

[41] H. O. Kreiss, J. Oliger, *Comparison of Accurate Methods for the Integration of Hyperbolic Equations*, Tellus XXIV **3** (1972)

[42] P. D. Lax, *Accuracy and resolution in the computation of solutions of linear and nonlinear equations*, in *Recent advances in Numerical Analysis, Proc. Symp.*, Mathematical Research Center, University of Wisconsin, Academic Press, pp. 107-117 (1978).

[43] H. Ma, *Chebyshev-Legendre Super Spectral Viscosity Method for Nonlinear Conservation Laws*, submitted to SIAM J. Numer. Anal.

[44] Y. Maday, S. Ould Kaber, E. Tadmor, *Legendre Pseudospectral Viscosity Method for Nonlinear Conservation Laws*, SIAM J. Numer. Anal. **30**, pp. 321-342 (1993)

[45] E. E. Meshkov, *Instability of the interface of two gases accelerated by a shock wave*, Izv. Akad. Nauk. SSSR Mekh. Zhidk. Gaza **4**, pp. 101-104 (1969)

[46] M. S. Min, S. M. Kaber, W. S. Don, *Fourier-Padé approximations and filtering for the spectral simulations of incompressible Boussinesq convection problem*, To appear in *J. Sci. Comput.*

[47] J. Norström, M. H. Carpenter, *High order finite difference methods, multidimensional linear problems and curvilinear coordinates*, Journal of Computational Physics, 148, pp. 621 (1999)

[48] J. Norström, M. H. Carpenter, *High-Order Finite Difference Methods, Multidimensional Linear Problems, and Curvilinear Coordinates*, Journal of Computational Physics, 173, pp. 149 (2001)

[49] H. Padé, *Mémoire sur les déveoppements en fractions continues de la fonction exponentielle puvant servir d'introduction à la théorie des fractions continues algébriques*, Ann. Fac. Sci. de l'Ec. Norm. Sup., 16, pp.395-436 (1899)

[50] A. Pumir, E. D. Siggia, *Development of singular solutions to the asysymmetric Euler equations*, Phys. Fluids A 4, 1472 (1992).

[51] M. D. Salas, S. Abarbanel, D. Gottlieb, *Multiple Steady States For Characteristic Initial Value Problems*, Applied Numerical Mathematics 2, pp. 193-210 (1986)

[52] E. B. Saff, R. S. Vargra, *Pade and rational approximation: Theory and application*, Academic press, Inc., New York, 1977.

[53] B. D. Shizgal, J. H. Jung, *On the resolution of the Gibbs phenomenon*, to appear

[54] C. W. Shu, S. Osher, *Efficient Implementation of Essentially Non-oscillatory Shock-Capturing Schemes, II*, J. Comp. Physics **83**, No. 1 pp. 32-78 (1989)

[55] C. W. Shu, P. Wong, *A note on the accuracy of spectral method applied to nonlinear conservation laws*, Journal of Scientific Computing, Vol 10, pp. 357-369 (1995)

[56] E. Tadmor, *Convergence of spectral methods for nonlinear conservation laws*, SINUM **26**, pp. 30-44 (1989)

[57] E. Tadmor, *Shock capturing by the spectral viscosity method*, Proceedings of ICOSAHOM 89, Elsevier Science Publishers B. V., North Holland, IMACS (1989)

[58] T. Tang, Z. Zhang, *Resolving small-scale structures in Boussinesq convection by adaptive grid methods*, 2003 (preprint).

[59] H. Vandeven, *Family of spectral filters for discontinuous problems*, Journal of Scientific Computing, 24, pp. 37-49 (1992)

[60] W. E, C. W. Shu, *Small-scale structures in Boussinesq convection*, Phys. Fluids 6(1) (1994)

[61] X. Zhang, J. A. Edwards, *The effect of trailing edge gometry on cavity flow oscillation driven by a supersonic shear layer*, Aeronautical Journal, 102-1013, pp. 129-136 (1998)